Enhanced photocatalytic and disinfection activities of silver loaded ordered mesoporous titanium dioxide for water treatment

Virender Singh Kundu*, Nikhil Chauhan & Suresh Kumar

Department of Electronic Science, Kurukshetra University, Kurukshetra 136 119, India

In the present paper ordered mesoporous titanium dioxide (TiO_2) has been synthesized by using the nanocasting method with SBA-15 as a hard template and titanium alkoxide as the precursor. The silver has been loaded onto the obtained ordered mesoporous TiO_2 using photoreduction method. The physicochemical properties of as-prepared and calcined silver loaded mesoporous titanium dioxide (SMTO) have been characterized by various techniques. The XRD pattern confirms the existence of tetragonal anatase-rutile mixed phases of TiO_2 with a crystallite size of the range of 12-15 nm. SEM and TEM images show that the aggregation of nanocrystalline phase results in the formation of nanometer sized mesoporous TiO_2 with a well-defined spherical morphology and retained ordered structure. The as-obtained samples exhibit good photocatalytic degradation of rhodamine B, Congo red and methyl orange dyes as model water contaminant at room temperature with UV light irradiation. The samples under study also show substantial disinfection properties against *E. coli & S. aureus* used as a model strain. The significant enhancement of the photocatalytic and disinfection activities of the SMTO materials is mainly attributed to their absorbed more photons and reduced electron-hole pair recombination due to synergic effect of porosity of the ordered structure and Ag-impregnated nanoparticles, respectively.

Keywords: Mesoporous TiO_2, Ag nanoparticles, XRD, SEM, TEM, Photocatalytic, Disinfection activities

1 Introduction

Semiconductor based photocatalytic oxidation and reduction offer a promising alternative for removing the organic and inorganic contaminant from wastewater[1-4]. Titanium dioxide is one of the most attractive semiconductors for years, for their photocatalytic reactions because of its high chemical stability, non-toxicity and low cost[5-8]. Its wide band gap energy (*E*g, 3.0-3.2 eV) allows absorption of UV light, generating electrons (e⁻) and holes (h⁺), which can subsequently induce redox reactions which in turn generate reactive oxygen spices (ROS) responsible for the photocatalytic destruction of contaminants in

TiO_2 further enhances its utility due to high crystallinity, large surface area and its ability to form regular and uniform nano-channel that can be accessed by external materials[10]. Since the discovery of ordered mesoporous silica (MCM-41 and SBA-15) in 1990's, the mesoporous material has attracted more and more interest due to their fascinating properties of tunable large pore size and pore area, high surface area[11]. During last decades, a great effort has been made to develop highly efficient photocatalysis for water

purification. A good photocatalyst should have high crystallinity and large surface area. The high crystallinity of the photocatalyst is desirable due to the decrease in defects which acts as recombination centers for photogenerated carriers. The large surface area is desired because it can provide more adsorption and reactive sites. Crystalline mesoporous anatase prepared by hard template such as SBA-15, KIT-6 had exhibited superior photocatalytic activity[12]. In general, mesoporous particles with a spherical shape and controlled size are more useful in catalysis, sorption media, and porous membrane etc[13]. Mesoporous TiO_2 had been widely studied as an efficient catalyst because ... e and high surface to volume ratio and also high photocatalytic activity[14]. The loading/deposition of metal nanoparticles with a large work function, such as Ag, Au, and Pt onto the surface of TiO_2 had been found effectively impede the e⁻- h⁺ recombination because of the Schottky barrier formed at the metal-semiconductor interface[15,16]. The decrease in carrier (electron-hole) recombination will further reinforce the photocatalytic activity of the material.

Various approaches to the synthesis of mesoporous TiO_2 with spherical morphology have been discussed. Kim *et al.*[17] synthesized monodispersed spherical

*Corresponding author (E-mail: vskundu_kuk@rediffmail.com)

mesoporous TiO₂ particles with the sol-gel approach with a soft template. The BET and BJH analysis show that the sample area and average pore size of the mesoporous TiO₂ increase with an increase in calcination temperature[17]. Zhang et al.[10] synthesized crystalline mesoporous anatase TiO₂ using the nanocasting method with KIT-6 as the hard template. The material with the high surface area of 207 m²/g was obtained. The study indicates that hard template synthesis method may work an effective method for efficient photolysis[10]. Olsen et al.[14] investigated that the dopants like Al, La, Si, and Zr increase the surface area and thermal stability of anatase mesoporous TiO₂ through structural modification and grain growth inhibition[14]. Wang et al.[18] observed that the single-crystal ordered mesoporous TiO₂ exhibited much higher activity than the polycrystalline TiO₂ since the high crystallization degree favored the transfer of photoelectrons, which might diminish their rate of recombination with holes. Also, found that TiO₂ with ordered mesoporous showed higher activity than that with disordered mesoporous, and the 3D ordered mesoporous channels were more favorable for photocatalytic oxidation than the 2D ordered mesoporous channels[18]. Liu et al.[5] investigated that photocatalytic tests of silver-modified TiO₂ microspheres reveals a much higher photocurrent and photocatalytic activity than that of other composites and pure TiO₂ microspheres[5]. However, the photocatalytic activities of silver-modified TiO₂ microspheres in aqueous suspension depend on the Ag loading process. Xiong et al.[15] synthesized mesoporous TiO₂ using a soft template and deposited silver on its surface using photoreduction method. The results show that the optimum Ag- loaded mesoporous TiO₂ may have highest Rh-B degradation and E. Coli disinfection[15].

In the present research paper, silver loaded ordered mesoporous TiO₂ is synthesized using photoreduction and nanoreplication, respectively. The three dyes rhodamine B (Rh B), congo red (CR) and methyl orange (MO), used as model water contaminant and E. coli & S. aureus used as probes to investigate the photocatalytic and disinfection properties of SMTO materials under UV light. The role of Ag loading on the catalytic performance of SMTO materials is also explored.

2 Experimental Details

2.1 Materials
Titanium tetra-isopropoxide (Ti{OCH(CH₃)₂}₄), poly (ethylene oxide)- poly (propylene oxide)- poly (ethylene oxide) triblock copolymer Pluronic P123 (EO₂₀PO₇₀EO₂₀), tetraethylorthosilane ((Si(OC₂H₅)₄; silica precursor), silver nitrate (AgNO₃), ethanol (C₂H₆O), NaOH, HCl, Rh B (C₂₈H₃₁C₁N₂O₃), MO(C₁₄H₁₄N₃NaO₃S) and CR (C₃₂H₂₂N₆Na₂O₆S₂) dyes were purchased from Sigma-Aldrich. All chemicals are of analytical grade and used without further purification.

2.2 Synthesis of SBA-15 mesoporous silica template
Mesoporous SBA-15 was prepared according to the well-established procedure outlined by Zhao et al.[19]. Highly viscous amphiphilic silicate solution 'tetraethylorthosilicate' (TEOS) was used as the silica source. Triblock copolymer P123 was used as the surface directing agent. In a typical procedure, the gel solution was prepared by dissolving 4 g of P123 in 80 g of 2M HCL and 20 g of de-ionized (DI) water under stirring before addition of 8.8 g of TEOS dropwise. The solution mixture was stirred at room temperature for 20 h and then aged for two overnights. The resulting solid was recovered by filtration, washed and air dried at room temperature. The calcination of pre dried solid was carried out by gradually increasing a temperature from ambient temperature to 500 °C in 8 h further heating at same the temperature for 6 h.

2.3 Synthesis of ordered mesoporous TiO₂ (MTO)
MTO was prepared by using titanium tetra-isopropoxide (TTIP) as a precursor. In a typical preparation, 1.0 g of TTIP was mixed with 50 mL of DI water. Their mixture giving white precipitates which were collected by centrifuge and decantation of the supernatant. The precipitates were dissolved in 1.1 g of HCl at ambient temperature. The clear solution of TiO₂ precursor was obtained which was dissolved in 1.0 g of the mesoporous silica templates by simple incipient wetness method[20]. The resulting combination was dried for 20 min at 150 °C. For maximum impregnation of TiO₂ precursor within the mesoporous of silica templates this impregnation–drying process is repeated ten times. The obtained composite was dried at 100 °C for one day. The same was then calcined at 450 °C for 4 h under ambient conditions. Lastly, the silica templates were removed from the composite by using 1 M NaOH solution. The residue was ordered mesoporous TiO₂.

2.4 Synthesis of silver loaded ordered mesoporous TiO₂ (SMTO)
The Ag nanoparticles were loaded/deposited onto the surface of ordered mesoporous TiO₂ using

photoreduction method[21]. 2.0 g of MTO was added in 500 mL of DI water. This mixture was sonicated for 20 min for getting a uniform suspension. The silver nitrate is then added to the suspension and stirred for 30 min in dark. The as obtained mixture was irradiated with a high pressure mercury vapour lamp of wavelength 280 nm for 3 h, giving whitish gray solid. The final product was collected, washed and dried at room temperature. The different loading concentration of Ag (*x* Ag; *x* is the weight percentage of Ag) was obtained by adding different volumes of silver nitrate solutions in MTO materials. The schematic illustration of the synthesis of SMTO material is shown in Fig. 1.

2.5 Characterization of Materials

The physicochemical properties of as obtained and calcined pure and SMTO materials were investigated by various characterization techniques. The crystal phase was identified by X-ray diffraction (XRD) using PANalytical X'Pert Pro diffractometer with CuKα (λ= 1.5406 Å) radiation at 45 kV and 40 mA over the 2θ range of 20-80°. The surface morphologies of samples are observed by using Zeiss Evo 40 analytical SEM. For morphological studies, the samples were mounted on an aluminum stub with the help of double adhesive carbon tape and coated with a layer of gold using Polaron SC7640 sputter coater. The surface elemental composition was analyzed using an energy dispersive X-ray spectrometer (EDX) attached to the SEM. The TEM characterization was carried out using Hitachi (H-7500) microscope at an accelerating voltage of 200 kV. Samples for TEM characterization were prepared by sonicating the SMTO material in ethanol for 30 min and evaporating a drop of the resulting suspension onto a holey carbon-coated film supported on a copper grid. The samples were viewed at different magnifications.

Fig. 1 — Schematic illustration of the synthesis of SMTO material.

N_2 adsorption–desorption isotherm analysis was measured at 77 K on a Micromeritics ASAP2010 volumetric adsorption analyzer. Prior to the measurement, the samples were degassed at 150 °C for 3 h. The total pore volume was determined from the sorption isotherms at $P/P_0 = 0.977$ and the specific surface area were calculated using the BET (Brunauer–Emmett–Teller) method from a range (P/P_0) of 0.05–0.2.

2.6 Photo catalytic degradation of Rh B, CR and MO dyes

Separate experiments were conducted for the investigation of photocatalytic degradation of Rh-B, CR, and MO dyes. For each experiment, initially, a suspension of 60 mL of 10^{-4} mol/liter concentration of individual dye was prepared with 0.05 g of the solid photocatalyst. The good quality of suspension was obtained by stirring and sonicating (20 min each) it in dark condition. The suspension was then irradiated with a 160 W high-pressure mercury lamp as UV light source (wavelength 280 nm). 10 mL of suspension was withdrawn at a uniform time interval of 20 min. The sampled liquid was then centrifuged and filtered. The filtered samples were analyzed using a Perkin Elmer Lambda 20 UV-Vis spectrophotometer.

2.7 Photocatalytic disinfection of *E. coli* and *S. aureus*

Two different bacterial strains *E. coli* (Gram –ve) & *S. aureus* (Gram +ve) were used to test the antimicrobial activity. The antibacterial assays were carried out in a sterilized 100 mL of conical glass flask containing 10 mL of nutrient broth. The culture medium was inoculated with 1.7×10^5 CFU/mL of *E. coli* and 2.3×10^5 CFU/mL of *S. aureus* bacterial culture and incubated in Remi CIS 24 plus incubator. The as obtained SMTO photocatalysts were added at a concentration of 1 mg/mL each, separately, in conical glass flasks. The prepared suspensions were irradiated with 8 W black light (as ultraviolet light source) for various time periods, i.e., 25, 50, 75 and 100 minutes. 100 μl inoculum of each treated bacterium were taken with physio care an Eppendorf micropipette and spread on nutrient agar plate using sterile L-rod. All the plates were kept for incubation at 37 ºC for 24 h. The formed colonies were counted and used to calculate the number of active cells. The control experiments were conducted without using the photocatalyst.

3 Results and Discussion

3.1 Crystal structure and characteristic of SMTO materials

X-ray powder diffraction patterns of crystalline SMTO (Ag=0, 1.0, 2.0 and 3.0) materials at room

temperature are presented in Fig. 2 and show the presence of anatase, rutile and silver peaks. These XRD patterns correspond to the tetragonal anatase-rutile mixed phase of TiO_2 with space group I41/amd (JCPDS 71–1166) for anatase and P42/mnm (JCPDS 72–1148) for rutile phase[22,23]. The quantitative analysis from the Gaussian fitting of diffraction peaks of XRD data[24] shows that there are 82.19% rutile, 15.24% anatase and almost 1.92% silver. The diffraction peaks for anatase correspond to planes (101), (200) and (202). The XRD peaks corresponding to rutile structure are (110), (101), (111), (210), (211), (220), (301) and (112). The presence of peaks corresponding to silver crystal planes (111) and (220) is the signature of the presence of Ag in SMTO material. The sharp diffraction peaks manifested show that the materials under consideration have high crystallinity. The crystallite size (D) of the samples was calculated from the width of the XRD peaks, using the Scherrer formula[25]:

$$D = 0.94 \, \lambda / \beta \cos \theta$$

where D is the average crystallite domain size perpendicular to the reflecting planes, λ is wavelength (0.15418 Å) of X-rays used, β is the broadening of diffraction line measured at half of its maximum intensity (in radian), full width at half maximum (FWHM), and θ is the diffraction angle. The average estimated crystallite size of the samples has been found to be 12-15 nm (derived from the FWHM of a peak corresponding to (110) plane) and listed in Table 1.

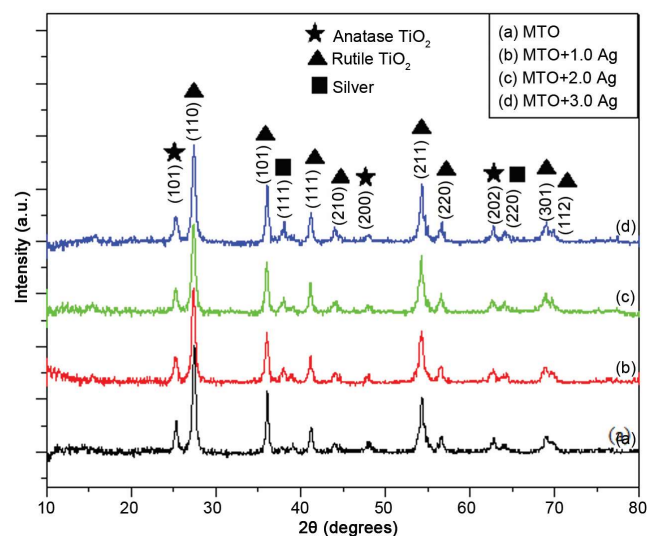To determine the particle size and morphology of the SMTO materials, SEM analysis was carried out.

Images as shown in Fig. 3(a, b) for 2.0 Ag sample, show that the particles have well defended spherical shape with sizes in the range 50-60 nm and that they are separated from each other with agglomeration; further pores can be seen. To further investigate the mesoporous structure of the materials, TEM of the same sample with Ag=2.0 was also carried out, as shown in Fig. 3(c). It shows that Ag nanoparticles are highly dispersed on the surface of SMTO materials. High level of dispersion of metal nanoparticles on the surface of TiO_2 is difficult to achieve with nanoporous materials[17]. TEM micrograph reveals

Table 1 — Surface area, pore diameter/size, pore volume and crystallite size of pure and Ag loaded TiO_2 nanostructures

Sample	BET Surface area (m²/g)	Pore volume[a] (cm²/g)	Pore size[b] (nm)	Crystallite size[c] (nm)
MTO	44.770	0.14	8.16	15
MTO +1.0Ag	80.89	0.15	4.66	14
MTO+2.0Ag	136.00	0.19	4.79	12
MTO+3.0Ag	87.80	0.15	5.02	15

[a] Total pore volume measured at $p/p_0 = 0.97$
[b] BJH average pore sizes calculated from desorption branch
[c] Crystallite size calculated by scherrer formula from XRD data

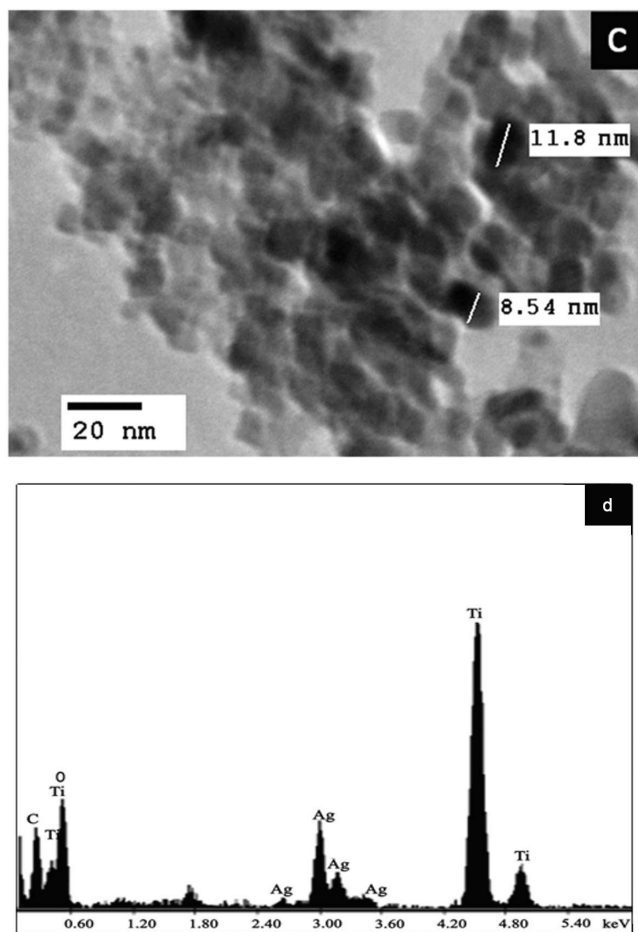Fig. 2 — XRD pattern of SMTO (Ag=0, 1.0, 2.0 and 3.0) materials.
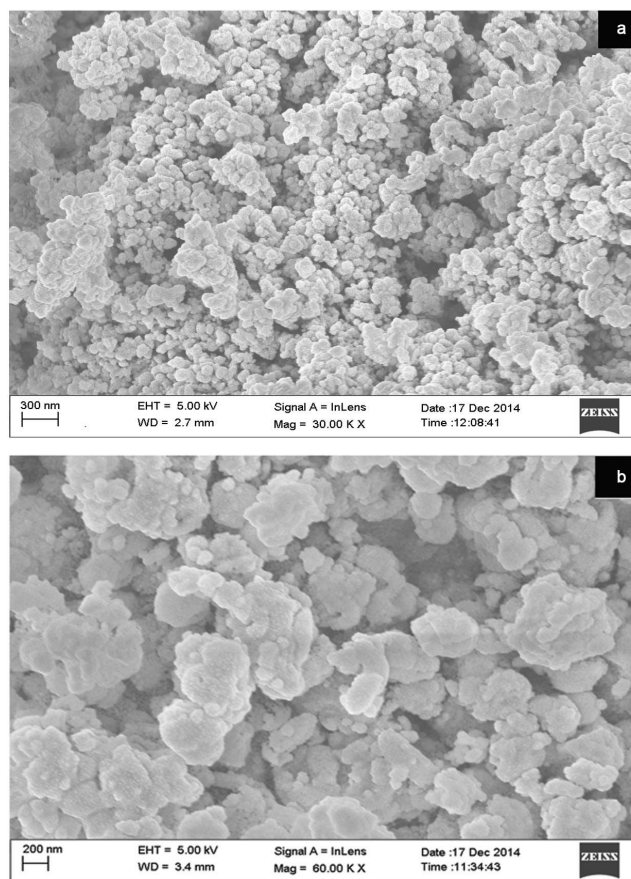
Fig. 3 — (a, b) SEM images at different magnifications, (c) TEM image and (d) EDX spectrum of SMTO (Ag=2.0) material.

crystalline particles of SMTO material in the range 12-15 nm (congruent with XRD measurements) with silver particles of average sizes 8-12 nm trapped in TiO_2 matrix. The spongy texture observed in the micrograph confirms the mesoporous nature of the sample. The TEM image also reveals the ordered hexagonal array of one dimensional mesoporous as a characteristic of SBA-15 support material.

The surface elemental composition of the various samples was estimated by EDX. The EDX spectra of the SIMTO (Ag = 2.0) material show signals directly related to the dopant (Fig. 3(d)). The spectrum shows that the sample under study mainly consists of Ti, Ag, and O, while C signals also originate from the substrate. The C signal comes from the conductive carbon film used as a support of the nanoparticles during SEM observation. The observed composition (at. %) of the elements from EDX spectrum of the sample under study is approximately same as target composition.

The porosity and pore size of SMTO materials were examined by BET analysis. The N_2 adsorption-desorption isotherm of all the samples under consideration show type IV curve with H2 hysteresis loop (Fig. 4(a-d)). This indicates a mesoporous feature of the samples. Type IV isotherm had a hysteresis loop due to capillary condensation of N_2 gas in the pores[26]. The hysteresis loops between adsorption and desorption curves, indicate the presence of ink bottle type pore structure with a narrow entrance and large cavity[27,28]. This type of hysteresis further indicated the presence of wide pore size distribution of the pores in the mesoporous samples. The BJH pore size distribution is shown in the inset of respective figures of Fig. 4.

The specific/surface area, pore volume and pore size of SMTO materials are summarized in Table 1. The pore size, estimated with BJH method from desorption branch is maximum for pure TiO_2 and decreases with increasing silver (Ag nanoparticles) doping. But the surface area of Ag-doped samples is larger than pure TiO_2. When the silver doping increased to 2.0 Ag, the sample had the highest surface area (136.00 (m^2/g)) and largest pore volume (0.19 (cm^2/g)).

3.2 Photocatalytic degradation performance

Photocatalytic degradation of dyes/pollutants in aqueous solutions using SMTO photocatalysts is assisted mainly by a series of hydroxylation reactions initiated by hydroxyl radicals[29-32] ($\cdot OH$). Upon UV light irradiation, electron-hole pairs are formed into the surface of the photocatalyst. Holes oxidize OH^- to $\cdot OH$ and electrons reacting with dissolved oxygen to form superoxide ions ($O_2{}^-\cdot$), which further react with water molecules to produce hydroxide ions (OH^-) and $\cdot OH$ radicals. These reactive $\cdot OH$ radicals are responsible for dye/pollutant degradation. Photocatalytic reaction mechanism of $\cdot OH$ generation by SMTO material against Rh-B dye is shown in Fig. 5.

The photocatalytic activity of SMTO materials was evaluated by degradation of three different dyes, i.e., Rh-B, CR, and MO as model water contaminant at room temperature with UV light irradiation were conducted. Figure 6(a-c) shows that the trend of photocatalytic activity the samples under study against all three dyes remain same. Pure TiO_2 shows minimum activity and Ag-loaded samples show higher photocatalytic activity for all the three dyes. Xiong *et al.*[15] also reported that Ag-doped mesoporous TiO_2 photocatalyst exhibit better photocatalytic activity
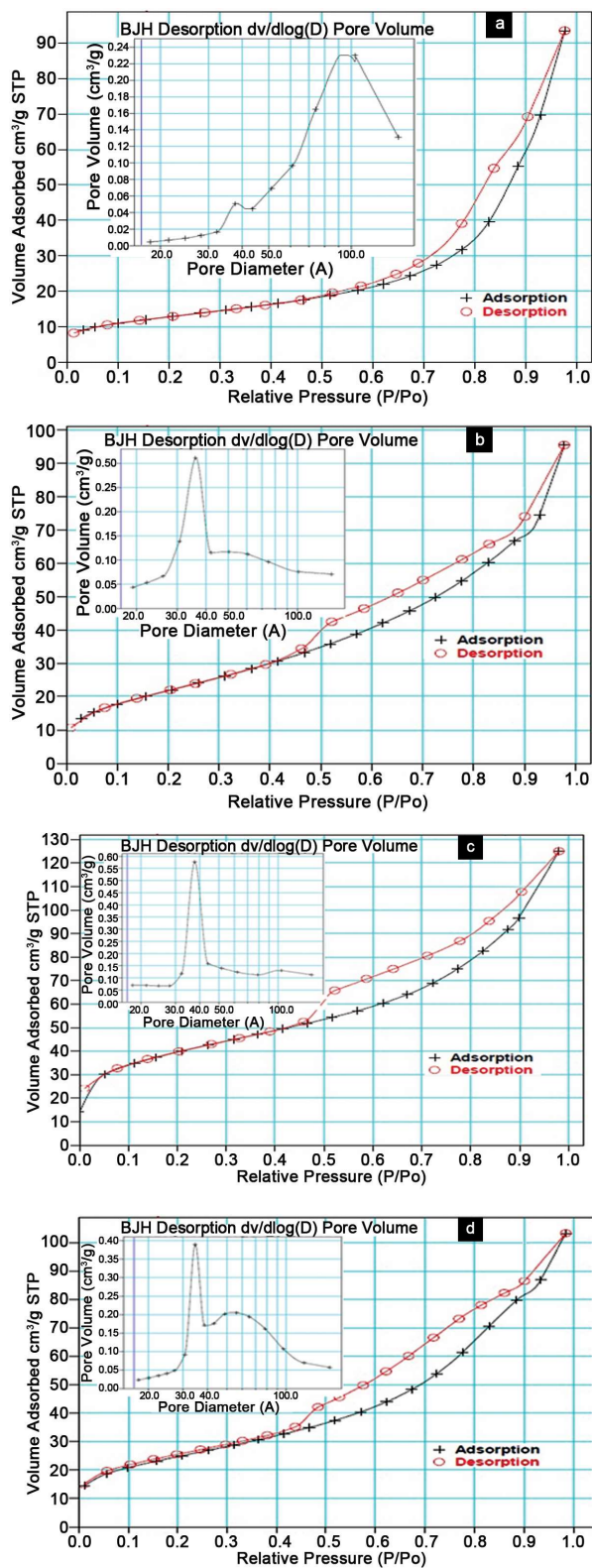
Fig. 4 — (a,d) N_2 adsorption-desorption isotherms for Ag=0, 1.0, 2.0 and 3.0 SMTO materials, respectively. Their corresponding BJH pore size distribution is shown in inset of respective figures.
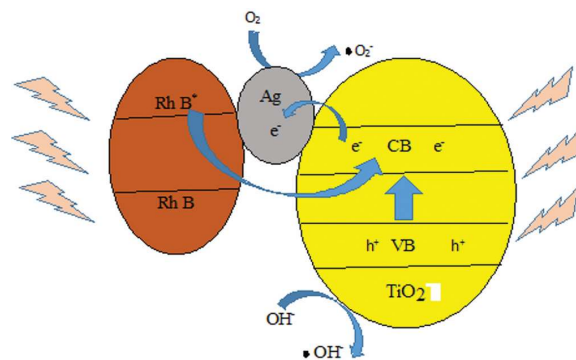

Fig. 5 — Photocatalytic reaction mechanism of SMTO material against Rh B.

compared to pure mesoporous TiO_2. The improvement is due to the increased oxygen defects concentration which can effectively help the separation of photogenerated electron - hole pair and extend the life of ●OH radicals. These two factors together account for the enhanced photocatalytic activity of Ag-loaded MTO as compared to pure MTO. The observed photocatalytic data could be satisfactorily described by pseudo-first-order model, and follow the first order kinetic equation; $\ln(C/C_0) = -k_{app}t$, where C_0 is the initial substrate concentration, C is the concentration at time 't' and k_{app} is the apparent first order equation rate. The calculated rate constants are plotted in Fig. 6(d).

SMTO materials show a different degree of degradation for different dyes (Table 2). They show best photocatalytic degradation against methyl orange (MO) dye, where almost complete (98%) degradation is achieved in 100 min by 2.0 Ag sample. The 2.0 Ag-loaded SMTO materials show maximum efficiency against all the dyes under consideration. The higher photocatalytic activity of this material can be explained in terms of large surface area, high pore volume and small crystallite size. The larger surface area and pore volume are likely to enhance photocatalytic activity by providing more active sites[33]. The 2.0 Ag SMTO material has highest surface area (136.00 (m^2/g)) and largest pore volume (0.19 (cm^2/g)). The crystallite size is also an important factor that influences the photocatalytic activity. Smaller crystallite size has more powerful redox ability due to their large band gap[34]. The 2.0 Ag sample has a minimum crystallite size of 12 nm.

3.3 Photocatalytic disinfection performance

The disinfection performance of the photocatalysts was studied using *E. coli & S. aureus* as a model strain. In the presence of TiO_2 photocatalysts under ultra-violet light, the number of viable *E. coli &*
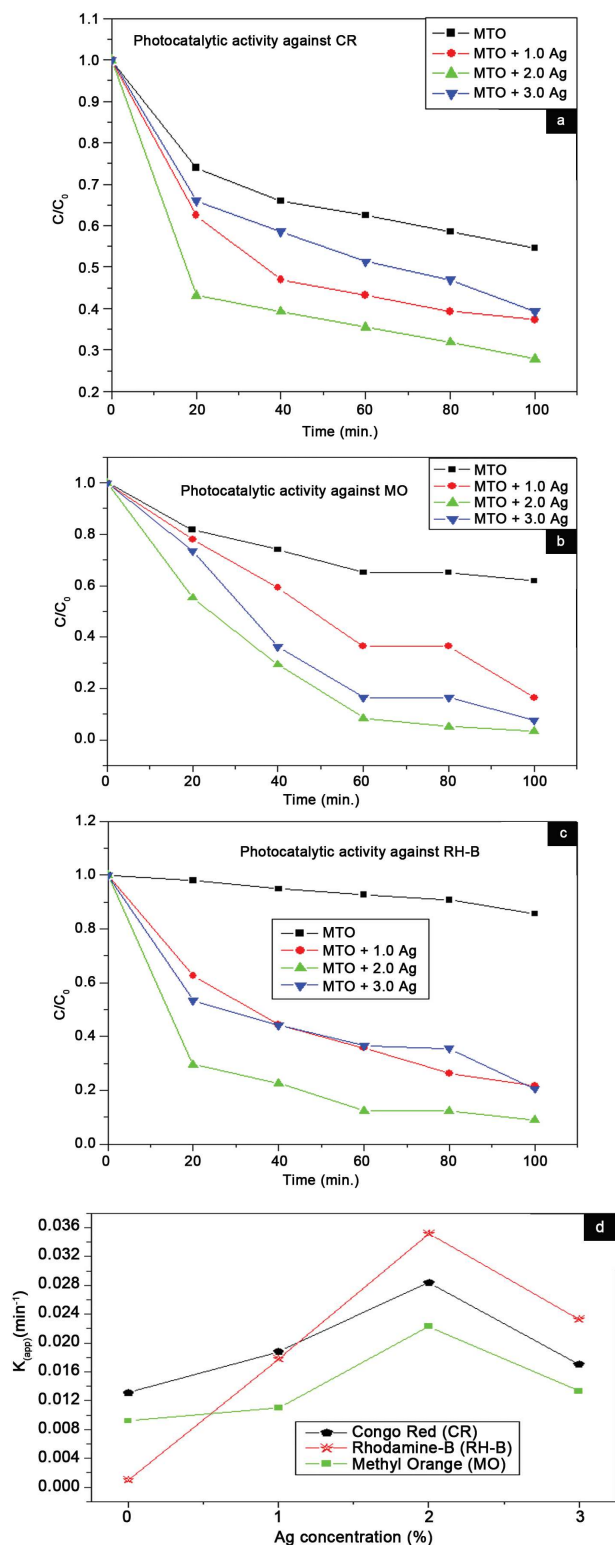
Fig. 6 — Photocatalytic degradation of (a) Congo red, (b) Methyl orange, (c) Rhodamine B dyes under UV light by SMTO materials and (d) apparent rate constant as a function of material composition.

Table 2 — Degradation of dyes after exposure to UV-Radiation

Samples	Percentage degradation of various dyes after 100 min of UV exposure		
	Congo red (CR)	Rhodamine-B (Rh-B)	Methyl Orange (MO)
MTO	41%	15%	42%
MTO+1.0Ag	63%	78%	84%
MTO+2.0Ag	73%	91%	98%
MTO+3.0Ag	61%	80%	93%

S. aureus cells decreased continuously with time (Figs 7 and 8). The antibacterial activity found to depends on the concentration of silver loading.

It is observed from the Fig. 8(a, b) that antibacterial activity of the present samples against both tested bacteria increased with Ag concentration and 3.0 Ag SMTO sample shows maximum antibacterial activity among all the four samples and pure MTO sample shows minimum activity. Ag nanoparticles itself have their antimicrobial activity. Silver shows its antimicrobial properties due to attachment of Ag nanoparticles on the surface of the cell membrane. Silver is supposed to interfere with permeability and respiration functions of the cell[35,36]. Although the bactericidal mechanism of Ag nanoparticles remains to be fully understood[36]. When Ag is loaded onto the mesoporous TiO_2 surface the resulting SMTO material showed enhanced antibacterial property due to their large surface area, which provides better contact with microorganisms. The combination of Ag with mesoporous TiO_2 resulted in a synergic effect of their improved antibacterial and photocatalytic activity[35]. The photocatalytic disinfection process has also been widely investigated and it is found that the photocatalytic and antimicrobial properties are due to the formation of reactive oxygen species (ROS) which have the tendency to inactivate bacteria[38].

The SMTO material showed more photocatalytic activity on Gram-negative bacteria because Gram-positive bacteria have more peptidoglycan than Gram-negative in the cell wall, which is negatively charged, and more silver ions may get trapped to peptidoglycan in Gram-positive bacteria[39]. It is also observed that the percentage of viable bacteria exponentially reduced with respect to the increasing concentration of Ag in TiO_2. Based on these results, it can be concluded that as obtained SMTO material had significant antibacterial action on both of the Gram classes of bacteria and also suggest that the doping of metal and
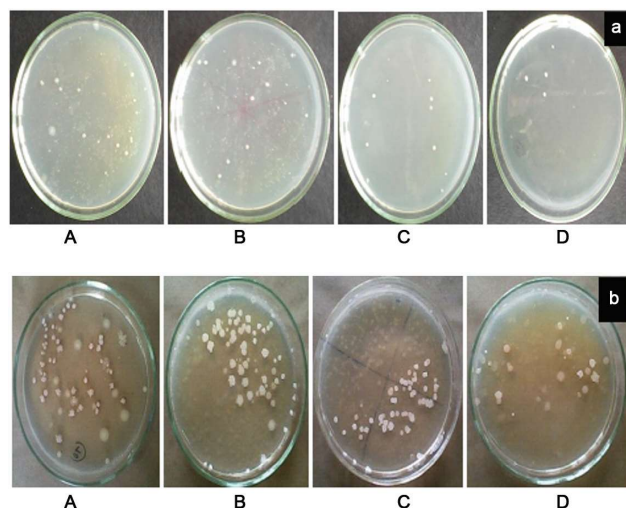
Fig. 7 — Antibacterial assay (a) *E. coli* and (b) *S. aureus*, colony count at 100 min, treated with pure MTO (A), 1.0 Ag SMTO (B), 2.0Ag SMTO (C) and 3.0 Ag SMTO (D).
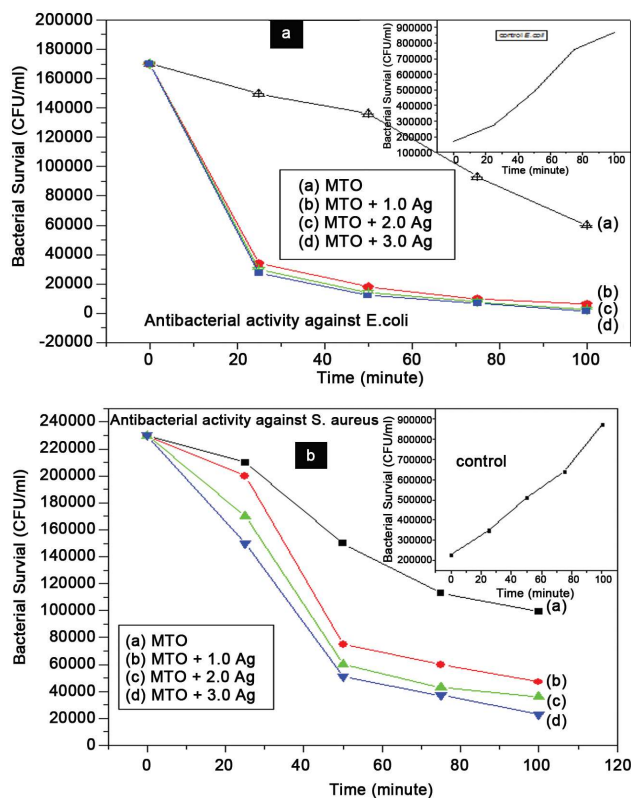

Fig. 8 — Antibacterial activity against (a) *E. coli* and (b) *S. aureus;* the control of the same is shown in inset of their respective figures.

metal oxides on the surface of TiO_2 nanoparticles increases the value of the e^-- h^+ charge separation by decreasing the band-gap energy, and leads to recombination delay and show good antibacterial activity[40]. The result obtained is consistent with already reported results[41,42].

4 Conclusions

Ordered mesoporous TiO_2 has been synthesized by using the nanocasting method with SBA-15 as hard template. The silver nanoparticles were loaded in the obtained ordered mesoporous TiO_2 using photoreduction method. The results indicate that SMTO materials have mesoporous structure and nanosized Ag particles are loaded/deposited onto the surface of mesoporous TiO_2. The XRD pattern confirms the existence of tetragonal anatase-rutile mixed phase of TiO_2 with crystallite size in the range of 12-15 nm. Electron morphologies show the aggregation of nano-meter sized mesoporous TiO_2 with a well-defined spherical morphology and retained ordered structure. The sample with 2.0 Ag had the highest surface area of 136.00 m^2/g and largest pore volume of 0.19 cm^2/g. The as-obtained samples exhibit good photocatalytic degradation of rhodamine B, Congo red and methyl orange dyes under UV light irradiation also shows substantial disinfection properties against *E. coli* & *S. aureus*. The significant improvement in the photocatalytic and disinfection activities of the SMTO materials is due to synergic effect of porosity of the ordered structure and Ag-impregnated/loaded nanoparticles.

References
1 Pirzada B M, Mir NA, Qutub N, Mehraj O, Sabir S & Muneer M, *Mater Sci Eng B*, 193 (2015) 137.
2 Zhang W, Tu G, Zhang H, Zheng Y & Yang L, *Mater Lett*, 114 (2014) 119.
3 Pant H R, Pant B, Sharma R K, Amarjargal A, Kim H J, Park C H, Tijing L D & Kim C S, *Ceram Int*, 39 (2013) 1503.
4 Zhou X, Li Y & Zhao Y, *RSC Adv*, 30 (2014) 15620.
5 Liu H, Dong X, Liu T & Zhu Z, *Sol Energy Mater Sol Cells*, 132 (2015) 86.
6 Fujishima A & Honda K, *Nature*, 238 (1972) 37.
7 Hoffmann M R, Martin ST, Choi W Y & Bahnemann D W, *Chem Rev*, 95 (1995) 69.
8 Yu J G & Zhang J, *Dalton Trans,* 39 (2010) 5860.
9 Kuvarega A T, Krause R W M & Mamba B B, *J Phys Chem C*, 115 (2011) 22110.
10 Zhang Z, Zuo F & Feng P, *J Mater Chem*, 20 (2010) 2206.
11 Corma A, *Chem Rev*, 97 (1997) 2373.
12 Bian Z F, Zhu J, Wen J, Cao F L, Huo Y N, Qian X F, Cao Y, Shen M Q, Li H X & Lu Y F, *Angew Chem*, 50 (2011) 1105.
13 Ren Y, Zhen M & Bruce P G, *Chem Soc Rev*, 41 (2012) 4909.

14 Olsen R E, Bartholomew C H, Huang B, Simmons C & Woodfield B F, *Micropor Mesopor Mater*, 184 (2014) 157.

15 Xiong Z, Ma J, Ng W J, Waite T D & Zhao X S, *Water Res*, 45 (2011) 2095.

16 Li H X, Bian Z F, Zhu J, Huo Y N, Li H & Lu Y F, *J Am Chem Soc*, 129 (2007) 4538.

17 Kim D S, Jeon J D & Shin K H, *Micropor Mesopor Mater*, 181 (2013) 61.

18 Wang J, Bian Z, Zhu J, Li H Wang J G, Bian Z F, Zhu J & Li H X, *J Mater Chem A*, 1 (2013) 1296.

19 Zhao D Y, Huo Q S, Feng J L, Chmelka B F & Stucky G D, *J Am Chem Soc*, 120 (1998) 6024.

20 Kim S S, Lee H K, Shon J K, Hur J Y, Kang M S, Park S S, Kong S S, Yu J A, Li D, Thakur S S & Kim J M, *Chem Lett*, 37 (2008) 140.

21 Tran H, Scott J, Chiang K & Amal R, *J Photochem Photobio A Chem*, 183 (2006) 41.

22 Peters G & Vill V, *Index of modern inorganic compounds*, *Sub volume A,* (Verlag: Berlin), 1989.

23 Choudhury B & Choudhury A, *Int Nano Lett*, 3 (2013) 55.

24 Li W, Ni C, Lin H, Huang C P & Shah S I, *J Appl Phys*, 96 (2004) 6663.

25 Klug H P & Alexander L E, *X-ray diffraction procedures for polycrystalline and amorphous materials*, (Wiley: New York), 1954.

26 Ma Y, Xing M, Zhang J, Tian B & Chen F, *Micropor Mesopor Mater,* 156 (2012) 145.

27 Sing K S W, Everett D H, Haul R A W, Moscow L, Ppierotti R A, Rouquerio & Seimieniewska T, *J Pure Appl Chem*, 57 (1985) 603.

28 Dumeignil F, Sato K, Imamura M, Matsubayashi N, Payen E & Shimada H, *Appl Catal A*, 241 (2003) 319.

29 Medana C, Calza P, Bello F D, Raso E, Minero C & Baiocchi C, *J Mass Spectrom*, 46 (2011) 24.

30 Lopez-Alvarez B, Torres-Palma R A & Penuela G, *J Hazard Mater*, 191 (2011) 196.

31 Stapleton D R, Konstantinou I K, Mantzavinos D, Hela D & Papadaki M, *Appl Catal B*, 69 (2010) 100.

32 An T C, An J B, Yang H, Li G Y, Feng H X & Nie X P, *J Hazard Mater*, 197 (2011) 229.

33 Wang Z, Mao L & Lin J, *J Photochem Photobiol A*, 177 (2006) 261.

34 Ohtani B, Ogawa Y & Nishimoto S I, *J Phys Chem B*, 101 (1997) 3746.

35 Liu Y, Wang X L, Yang F & Yang X R, *Micropor Mesopor Mater*, 114 (2008) 431.

36 Kvitek L, Panacek A, Soukupova J, Kolar M, Vecerova R, Prucek R, Holecova M & Zboril R, *J Phys Chem C*, 112 (2008) 5825.

37 Sharma V K, Yngard R A & Lin Y, *Adv Colloid Interfac*, 145 (2009) 83.

38 Chen F N, Yang X D & Wu Q, *Environ Sci Technol*, 43 (2009) 4606.

39 Kawahara K, Tsuruda K, Morishita M & Uchida M, *Dent Mater*, 16 (2000) 452.

40 Banerjee S, Gopal J, Muraleedharan P, Tyagi A K & Raj B, *Curr Sci*, 90 (2006) 1378.

41 Gupta K, Singh R P, Pandey A, Pandey A & Beilstein, *J Nanotechnol*, 4 (2013) 345.

42 Jurado1 Z V Q, Mendoza M A W, Bandin H M A, Leal E G V, González E C & Pérez E, *Mater Sci Appl*, 5 (2014) 895.